

¹ Supplementary Materials File

² Alejandro Damian-Serrano, Steven H.D. Haddock, Casey W. Dunn

³ Supplementary Methods

⁴ Phylogenetic inference: We aligned the sequences using MAFFT (1) (alignments available
⁵ in Dryad). We inferred a Maximum Likelihood (ML) phylogeny (S2) from 16S and 18S
⁶ ribosomal rRNA genes using IQTree (2) with 1000 bootstrap replicates (iqtree -s alignment.fa
⁷ -nt AUTO -bb 1000). We used ModelFinder (3) implemented in IQTree v1.5.5. to assess the
⁸ relative model fit. ModelFinder selected GTR+R4 for having the lowest Bayesian Information
⁹ Criterion score. Additionally, we inferred a Bayesian tree with each gene as an independent
¹⁰ partition in RevBayes (4) (S5), which was topologically congruent with the unconstrained
¹¹ ML tree. The *alpha* priors were selected to minimize prior load in site variation.

¹² Diet data curation: We removed the gelatinous prey observations for *Praya dubia* eating
¹³ a ctenophore and a hydromedusa, and for *Nanomia* sp. eating *Aegina* since we believe these
¹⁴ are rare events that have a much larger probability of being detected by ROV methods than
¹⁵ their usual prey, and it is not clear whether the medusae were attempting to prey upon
¹⁶ the siphonophores. Personal observations on feeding (from SHDH, CAC, and Philip Pugh)
¹⁷ were also included for *Resomia ornicephala*, *Lychnagalma utricularia*, *Bargmannia amoena*,
¹⁸ *Erenna richardi*, *Erenna laciniata*, *Erenna sirena*, and *Apolemia rubriversa*. The feeding
¹⁹ guilds declared in this study are: small-crustacean specialist (feeding mainly on copepods
²⁰ and ostracods), large crustacean specialist (feeding on large decapods, mysids, or krill), fish
²¹ specialist (feeding mainly on actinopterygian larvae, juveniles, or adults), gelatinous specialist
²² (feeding mainly on other siphonophores, medusae, ctenophores, salps, and/or doliolids), and
²³ generalist (feeding on a combination of the aforementioned taxa, without favoring any one
²⁴ prey group). These were selected to minimize the number of categories while keeping the
²⁵ most different types of prey separate.

26 Data wrangling for comparative analyses: For comparative analyses, we removed species
27 present in the tree but not represented in the morphology data, and *vice versa*. Although we
28 measured specimens labeled as *Nanomia bijuga* and *Nanomia cara*, we are not confident in
29 some of the species-level identifications, and some specimens were missing diagnostic zooids.
30 Thus, we decided to collapse these into a single taxonomic concept (*Nanomia* sp.). All
31 *Nanomia* sp. observations were matched to the phylogenetic position of *Nanomia bijuga* in
32 the tree. We carried out all phylogenetic comparative statistical analyses in the programming
33 environment R (5), using the Bayesian ultrametric species tree (S8), and incorporating
34 intraspecific variation estimated from the specimen data as standard error whenever the
35 analysis tool allowed it. R scripts and summarized species-collapsed data available in the
36 Dryad repository. For each character (or character pair) analyzed, we removed species
37 with missing data and reported the number of taxa included. We tested each character for
38 normality using the Shapiro-Wilk test (6), and log-transformed those that were non-normal.

39 Data wrangling for the variance-covariance analyses: When fitting all variance-covariance
40 terms simultaneously (S16-18), we selected the largest set of characters that would allow the
41 analysis to run without computational singularities. This excluded many of the morphometric
42 characters which are linearly dependent on other characters. Since the functions do not
43 tolerate missing data, we ran the analyses in two ways: One including all taxa but transforming
44 absent states to zeroes, and another removing the taxa with absent states. These analyses
45 could only be carried out on the subset of taxa for which diet data is available, and only
46 among character pairs that are not computationally singular for that taxonomic subset.
47 Gelatinous specialist correlations could only be estimated for a small subset of characters
48 present in *Apolemia* (S21F, S22E, S23D) and should be interpreted with care.

49 Comparative tools used to test character associations: To test for correlated evolution
50 among binary characters, we used Pagel's test (7). To characterize and evaluate the re-
51 lationship between continuous characters, we used phylogenetic generalized least squares
52 regressions (PGLS) (8). To compare the evolution of continuous characters with categorical

53 aspects of the diet, we carried out a phylogenetic logistic regression (R nlme::gls using the
54 ‘corBrownian’ function for the argument ‘correlation’).

55 DAPC optimization: Some taxa have inapplicable states for certain absent characters
56 (such as the length of a nematocyst subtype that is not present in a species), which are
57 problematic for DAPC analyses. We tackled this by transforming the absent states to
58 zeroes. This approach allows us to incorporate all the data, but creates an attraction bias
59 between small character states (*e.g.* small tentilla) and absent states (*e.g.* no tentilla).
60 Absent characters are likely to be very biologically relevant to prey capture and we believe
61 they should be accounted for in a predictive approach. We limited the number of linear
62 discriminant functions retained to the number of groupings in each case. We selected
63 the number of principal components retained using the a-score optimization function (R
64 adegenet::optim.a.score) (9) with 100 iterations, which yielded more stable results than the
65 cross validation function (R adegenet::xval). This optimization aims to find the compromise
66 value with highest discrimination power with the least overfitting. The discriminant analysis
67 for feeding guild (7 principal components, 4 discriminants) produced 100% discrimination,
68 and the highest loading contributions were found for the characters (ordered from highest
69 to lowest): Involucrum length, heteroneme volume, heteroneme number, total heteroneme
70 volume, tentacle width, heteroneme length, total nematocyst volume, and heteroneme width
71 (S10).

72 Supplementary Materials

73 Other trees inferred in this work include:

74 The constrained tree inferences utilized the following constrain topology:

2.1) Definitions of homologous structures used throughout this work.

Structure	Definition
Haploneme	Nematocyst with no shaft
Heteroneme	Nematocyst with a distinct shaft
Desmoneme	Small oval/tapered adhesive nematocyst with thick coiled tubule
Rhopaloneme	Small rod-like nematocyst found on the terminal filament
Terminal filament	Distal extension of the tentillum beyond the cnidoband
Cnidoband	Distinct packing of nematocysts on the dorsal side of the tentillum
Tentacle	Tubular projection from the gastrozooid basigaster
Tentillum	Evenly spaced dorsal evagination of the tentacle carrying ordered and functional nematocysts
Involucrum	Extension of the pedicle covering part of the cnidoband
Pedicle	Proximal region of the tentillum between the cnidoband and the tentacle
Elastic strand	Mesoglea derived collagenous double strand underlying the cnidoband of some siphonophores

2.2) Definitions of the continuous morphological and kinematic characters measured.

Character	Definition	Units
Cnidoband length	Distance from the base to the tip of the cnidoband in natural position	micrometers
Cnidoband free length	Distance from the base to the tip of the cnidoband when stretched straight	micrometers
Cnidoband width	Diameter of the cnidoband on the widest point	micrometers
Involucrum length	Length of the involucrum from the base of the cnidoband to its most distal extent	micrometers
Heteroneme length	Length of the heteronemes	micrometers
Heteroneme width	Diameter of the heteronemes at the widest point	micrometers
Heteroneme shaft length	Length of the heteroneme shaft	micrometers
Heteroneme shaft width	Width of the heteroneme shaft	micrometers
Heteroneme number	Number of heteronemes in each tentillum (# in each row*2)	micrometers
Haploneme length	Length of the haplonemes	micrometers
Haploneme width	Diameter of the haplonemes at the widest point	micrometers
Rhopaloneme length	Length of the rhopalonemes	micrometers
Rhopaloneme width	Diameter of the rhopalonemes at the widest point	micrometers
Desmoneme length	Length of the desmonemes	micrometers
Desmoneme width	Diameter of the cnidoband at the widest point	micrometers
Involucrum length	Length of the involucrum from the base of the cnidoband to its most distal extent	micrometers
Elastic strand width	Diameter of the descending elastic strand at the widest point	micrometers
Pedicle width	Diameter of the pedicle	micrometers
Tentacle width	Diameter of the tentacle	micrometers
Haploneme row number	Number of haploneme rows running parallel to the length of the cnidoband	micrometers
Cnidoband coiledness	Cnidoband free length / Cnidoband length	adimensional
Heteroneme elongation	Heteroneme Length/Width	adimensional
Haploneme elongation	Haploneme Length/Width	adimensional
Desmoneme elongation	Desmoneme Length/Width	adimensional
Rhopaloneme elongation	Rhopaloneme Length/Width	adimensional
Heteroneme shaft extension	Heteroneme shaft length / Heteroneme capsule length	adimensional
Nematocyst Surface area	$4\pi^2((L\text{Length}^2)/(\text{Width}^2))^1.6 \times ((\text{Width}/2)^2)^1.6)/(3)^{1/1.6}$	micrometers squared
Nematocyst volume	Ellipsoid formula : $(4/3)\pi^1(L\text{Length}^2)(\text{Width}^2)^2$	micrometers cubed
Nematocyst SA/V ratio	Nematocyst surface area / Nematocyst volume	1/micrometers
Total haploneme volume	Haploneme volume * Haploneme row number * (Cnidoband free length / Haploneme width)	micrometers cubed
Total heteroneme volume	Heteroneme volume * Heteroneme number	micrometers cubed
Total nematocyst volume	Total haploneme volume + Total heteroneme volume	micrometers cubed
Total discharge time	Time from initial cnidoband movement to complete conformational change	milliseconds
Average CB discharge speed	Distance covered by the leading edge of the discharging cnidoband in the total discharge time.	mm/s
Maximum CB discharge speed	Maximum speed attained by the leading edge of the discharging cnidoband	mm/s
Heteroneme discharge speed AVG	Distance covered by the heteroneme nematocyst tubule from initial ejection to full eversion in the time it takes to evert fully	mm/s
Heteroneme discharge free speed AVG	Distance covered by the heteroneme nematocyst tubule in the time it takes to evert fully, accounting for coiling.	mm/s
Heteroneme discharge speed MAX	Maximum speed attained by the non-shaft tubule of the heteroneme nematocysts during eversion.	mm/s
Heteroneme discharge free speed MAX	Maximum speed attained by the non-shaft tube of the heteroneme nematocysts during eversion, accounting for coiling.	mm/s
Heteroneme shaft discharge speed MAX	Maximum speed attained by the shaft of the tubule of the heteroneme nematocysts during initial eversion.	mm/s
Heteroneme filament length	Distance covered by the heteroneme nematocyst tubule from initial ejection to full eversion	micrometers
Haploneme discharge speed AVG	Distance covered by the haploneme nematocyst tubule from initial ejection to full eversion in the time it takes to evert fully.	mm/s

Figure 1: Character definitions.



Figure 2: Maximum likelihood IQTree inference, unconstrained. Node labels are bootstrap support values.

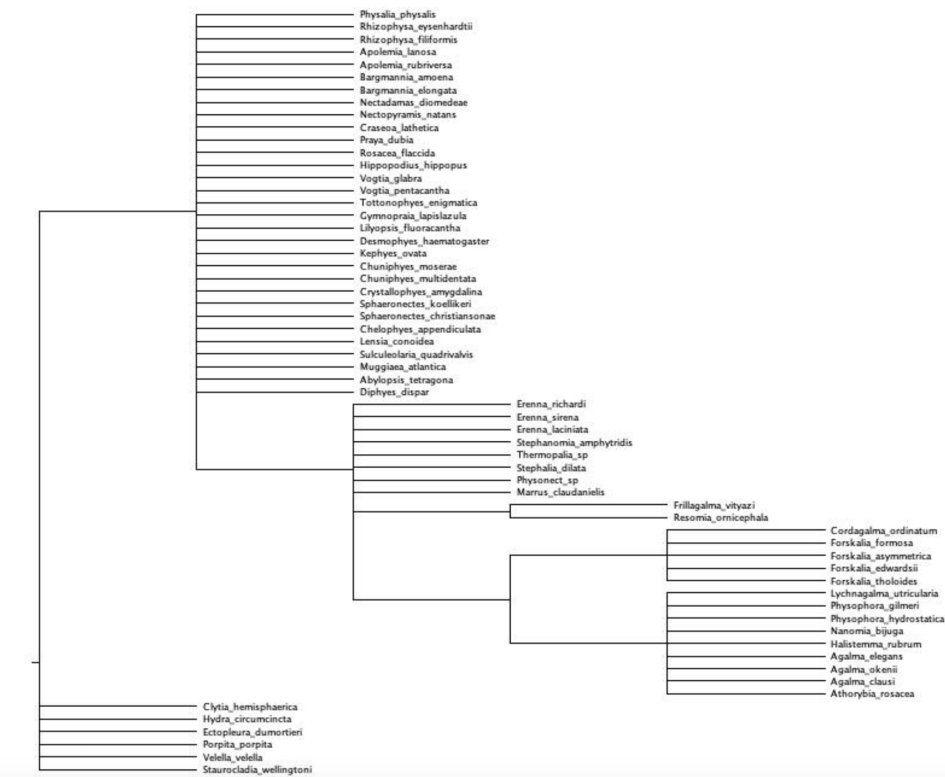


Figure 3: Topology used to constrain analyses (minimal topological statements based on the incongruences between the unconstrained tree and Munro et al. (2018)).

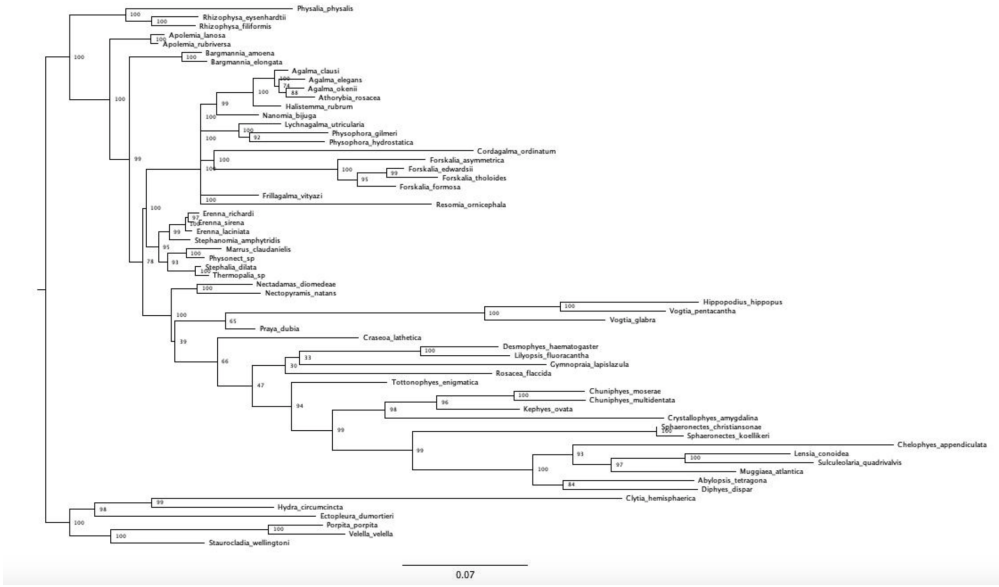


Figure 4: Constrained IQTree ML inference. Node labels are bootstrap support values.

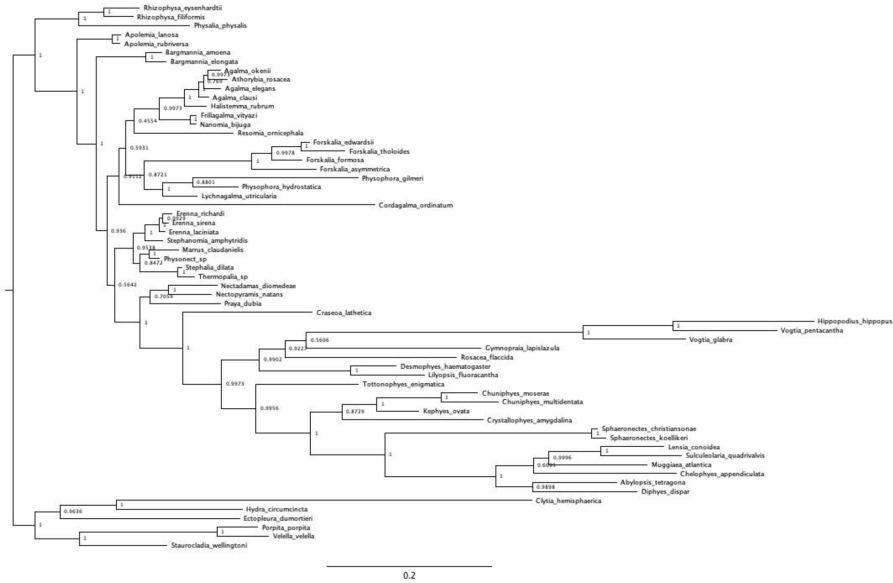


Figure 5: Unconstrained Bayesian topology inference in RevBayes (node labels are Bayesian posteriors).

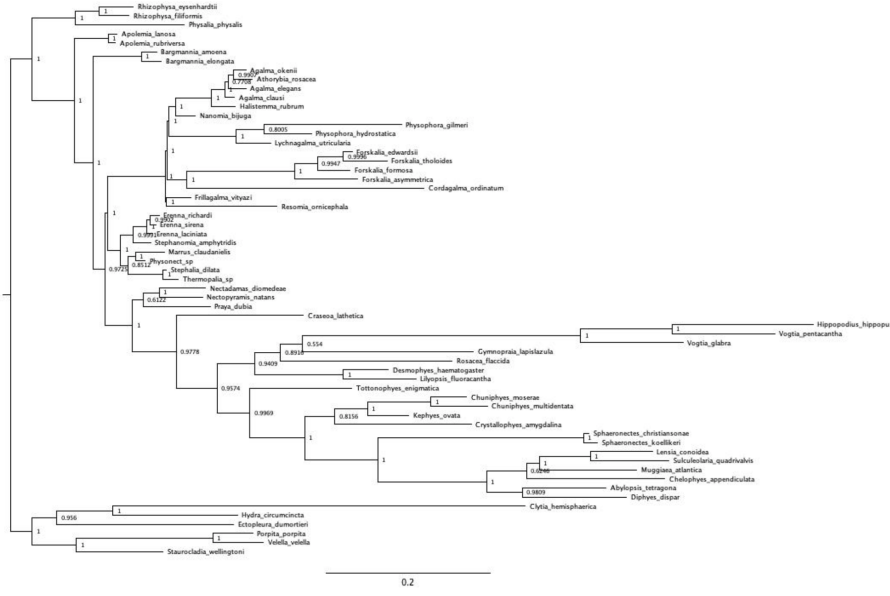


Figure 6: Clade constrained Bayesian inference in RevBayes (node labels are Bayesian posteriors).

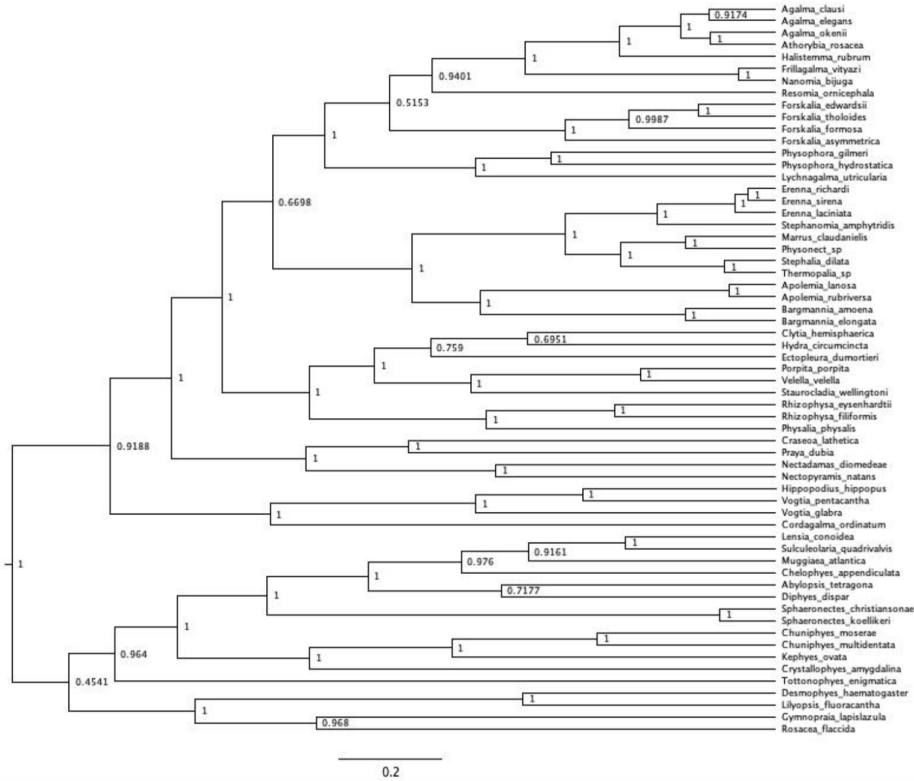


Figure 7: Unconstrained ultrametric Bayesian time tree branch length and topology inference in RevBayes (node labels are Bayesian posteriors). Arbitrary rooting.).

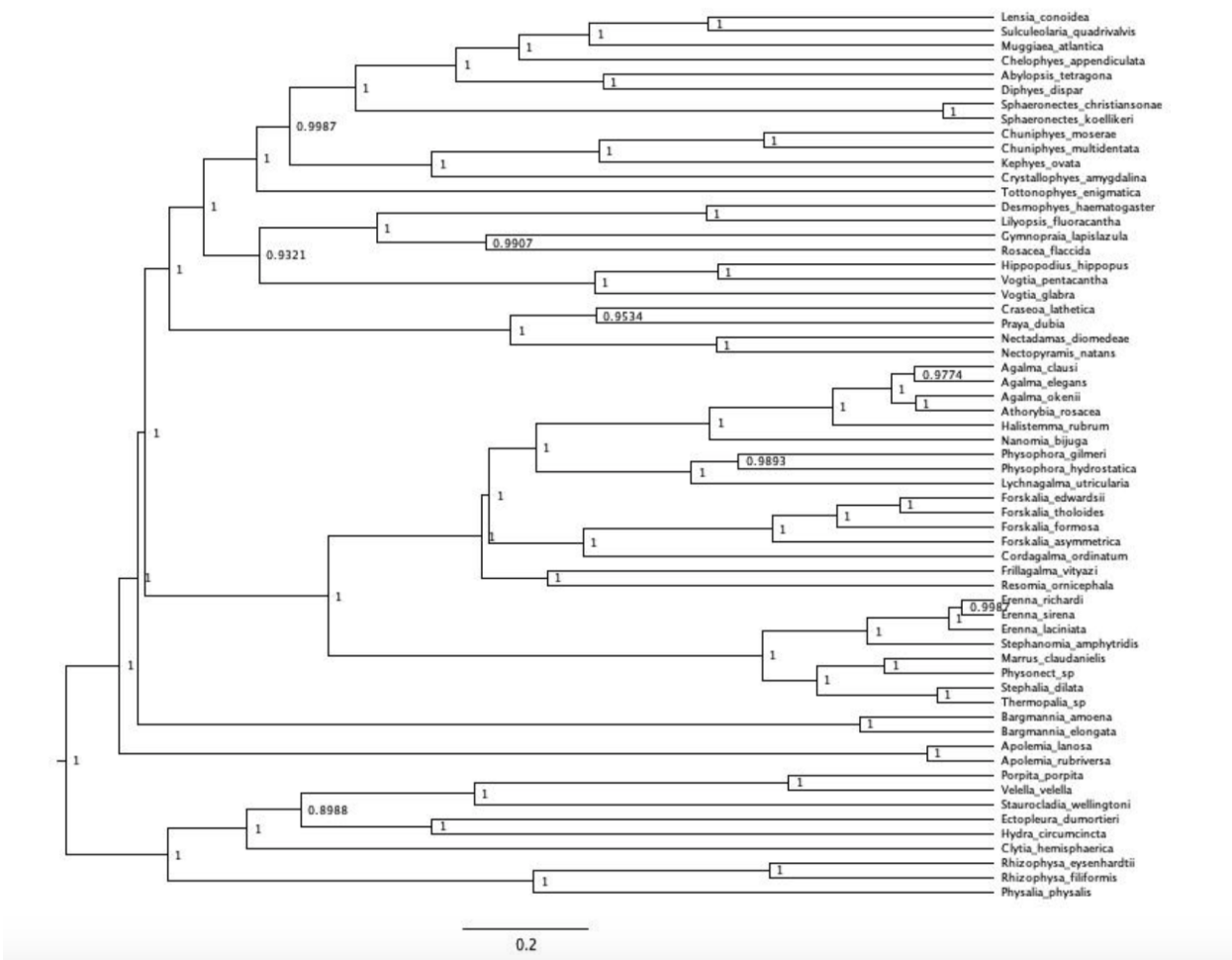


Figure 8: Ultrametric Bayesian time tree branch length inference in RevBayes (node labels are bayesian posteriors). Topology clamped to the Bayesian constrained topology inference in @ref{Bayes_constrained}. Tree rooted using outgroup constraint.

DAPC discriminant analyses:

Character	N	dAICc BM	dAICc OU1	dAICc OUm	Msig	Cvar	Svar	Sasr	Shgt	Dcfid	
Haploneme elongation	21	0	0.953	713.671	0.801	0	0.038	0.156	0.362	0.098	
Heteroneme shaft width μm	19	0	1.051	632.503	0.767	0.801	0.128	0.092	0.4	0.813	
Cnidoband width μm	21	0	1.595	761.241	0.781	0.723	0.072	0.09	0.31	0.228	
Heteroneme shaft free length μm	19	0	1.649	628.334	0.791	0.402	0.941	0.098	0.575	0.464	
Heteroneme volume μm^3	19	0	2.105	629.21	0.779	0.034	0.39	0.338	0.637	0.392	
Haploneme width μm	21	0	2.452	766.546	0.779	0.599	0.316	0.791	0.995	0.288	
Pedicle width μm	21	0	2.458	764.406	0.815	0.791	0.368	0.26	0.963	0.298	
Heteroneme width μm	19	0	2.516	634.229	0.805	0.809	0.292	0.208	0.709	0.38	
Tentacle width μm	22	0	2.702	383.12	0.835	0.496	0.344	0.867	0.096	0.444	
Heteroneme to CB	19	0	0.127	NA		0.811	0.336	0.004	0.068	0.026	0.434
Haploneme surface area:volume	21	0	2.282	757.267	0.747	0.563	0.392	0.583	0.927	0.15	
Heteroneme elongation	19	0.217	0	618.621	0.819	0.601	0.012	0.707	0.062	0.715	
Total nematocyst volume	22	0.57	0	378.872	0.809	0.501	0.06	0.088	0.266	0.501	
Heteroneme free length μm	19	0.746	0	627.372	0.811	0.885	0.593	0.156	0.368	0.679	
Total haploneme volume	21	1.281	0	730.592	0.829	0.452	0.038	0.134	0.096	0.819	
Cnidoband length μm	21	1.439	0	763.478	0.761	0.328	0.04	0.11	0.098	0.803	
Cnidoband free length μm	21	2.219	0	760.518	0.843	0.35	0.012	0.066	0.05	0.911	
Cnidoband coiledness	21	2.669	0	765.921	0.807	0.002	0.008	0.03	0.076	0.791	
Haploneme row number	21	4.177	0	729.95	0.825	0.004	0.002	0.06	0.006	0.346	
Haploneme free length μm	21	5.497	0	778.011	0.793	0.388	0.032	0	0.052	0.306	
Heteroneme shaft extension	19	6.17	0	611.533	0.775	0	0.068	0.665	0.124	0.184	
Rhopaloneme elongation	13	144.229	146.783	0	0.753	0.641	0.434	0.188	0.933	0.617	
Desmoneme length μm	13	148.14	151.403	0	0.763	0.182	0.607	0.31	0.745	0.014	
Rhopaloneme length μm	13	150.731	154.198	0	0.739	0.803	0.24	0.03	0.14	0.316	
Rhopaloneme width μm	13	150.82	154.287	0	0.743	0.462	0.306	0.07	0.182	0.092	
Desmoneme elongation	13	159.594	158.584	0	0.719	0.206	0.074	0.094	0.036	0.993	
Desmoneme width μm	13	164.639	168.106	0	0.773	0.11	0.885	0.098	0.605	0.002	
Involucrum length μm	14	148.672	151.078	0	0.779	0.126	0.17	0.25	0.418	0.671	
Elastic strand width μm	15	473.984	477.156	0	0.827	0.921	0.184	0.064	0.953	0.785	
Total heteroneme volume	17	619.03	619.932	0	0.797	0.803	0.078	0.172	0.35	0.697	
Heteroneme number	17	620.836	620.193	0	0.777	0.39	0.008	0.074	0.056	0.054	

Brownian Motion Supported

Single Optimum OU Supported

Multiple Optima OU Supported

Figure 9: Model support (delta AICc) for each morphological character analyzed on the feeding guild reconstruction regime tree. OU1 = Single-optimum Ornstein-Uhlenbeck. OUm = Multi-optima Ornstein-Uhlenbeck. Model adequacy scores calculated for the best supported model only. Msig = mean of squared contrasts. Cvar = coefficient of variation of the absolute value of the contrasts. Svar = Slope of a linear model fitted to the absolute value of the contrasts against their expected variances. Sasr = slope of the contrasts against the ancestral state inferred at each corresponding node. Shgt = slope of the contrasts against node depth. Dcfid = Kolmogorov-Smirnov D-statistic comparing contrasts to a normal distribution with SD equal to the root of the mean of squared contrasts.

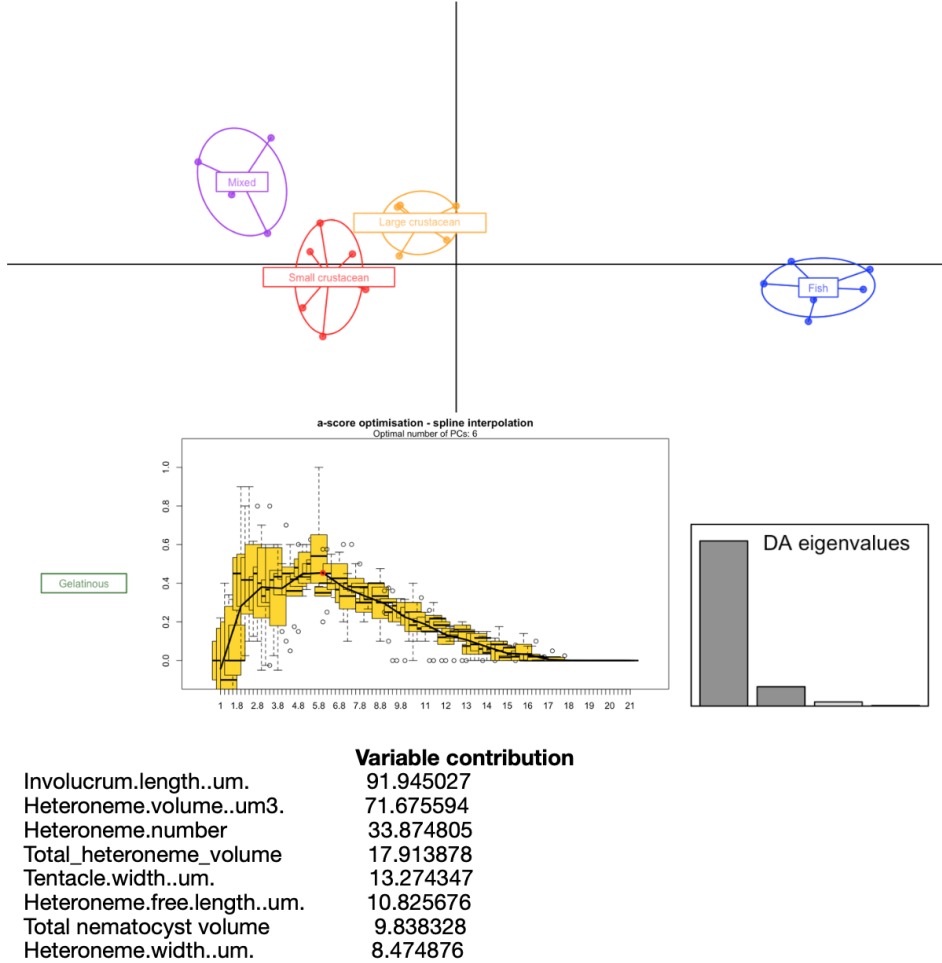
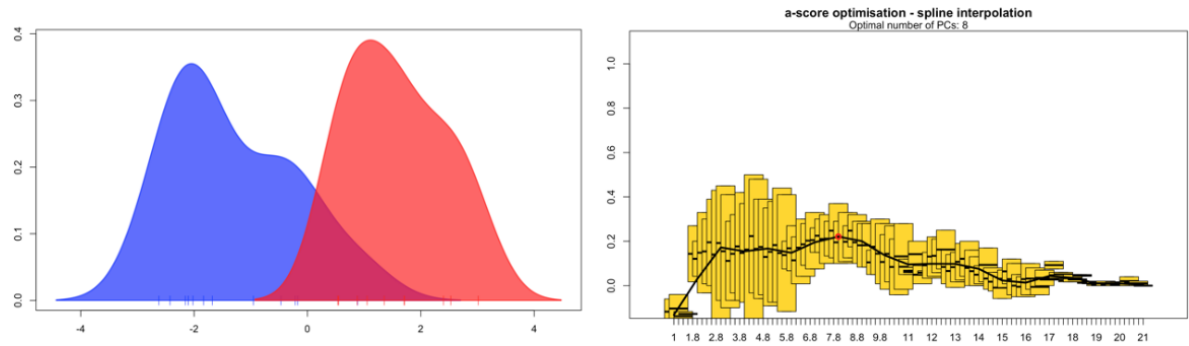


Figure 10: DAPC for Feeding guilds. Six PCs retained after a-score optimization (100 iterations). Four LDA functions used. Discriminant power on training set: 100%. Prediction posterior distribution heat map in main text Figure 6. Variable contribution (top quartile) calculated by the sum of the LDA variable loadings weighted by the eigenvalue of each LDA.



Variable contribution

Total_nematocyst_volume	12.810953
Tentacle.width..um.	5.687086
haploneme_elongation	4.586386
SAV_haploneme	4.264843
Haploneme.row.number..um.	2.966009
Cnidoband.length..um.	1.959479
Cnidoband.width..um.	1.679753
Cnidoband.free.length..um.	1.468262

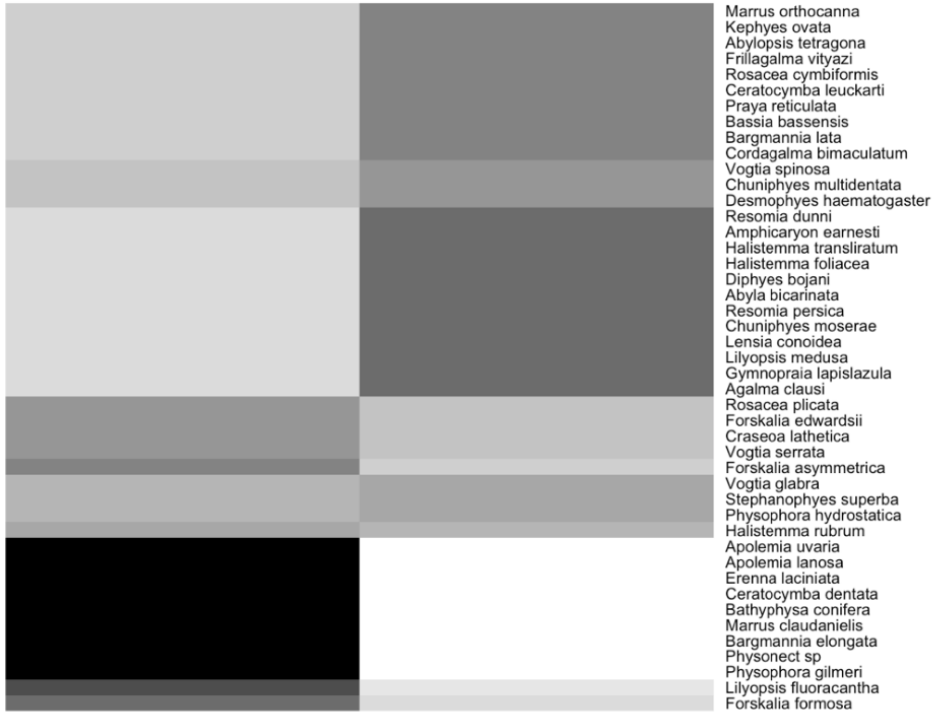
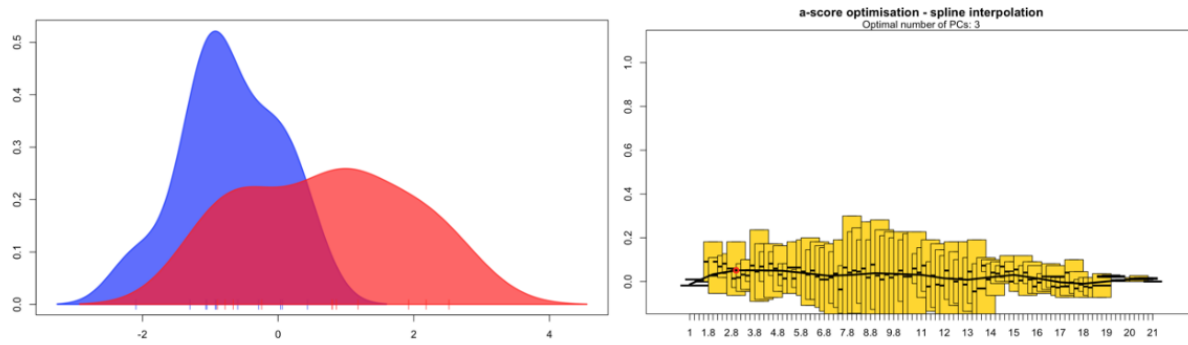


Figure 11: DAPC for copepod presence in the diet. Eight PCs retained after a-score optimization (100 iterations). One LDA functions used. Discriminant power on training set: 95.4%. Grayscale heat map shows the posterior probability distribution of the predictions. Variable contribution (top quartile) calculated by the sum of the LDA variable loadings weighted by the eigenvalue of each LDA.



Variable contribution

total_haploneme_volume	2.2734508
Heteroneme.volume..um3.	1.1308252
total_nematocyst_volume	1.1104459
total_heteroneme_volume	0.9402038
Cnidoband.length..um.	0.7583124
Cnidoband.free.length..um.	0.6650068
Involucrum.length..um.	0.6097537
Pedicle.width..um.	0.5447312

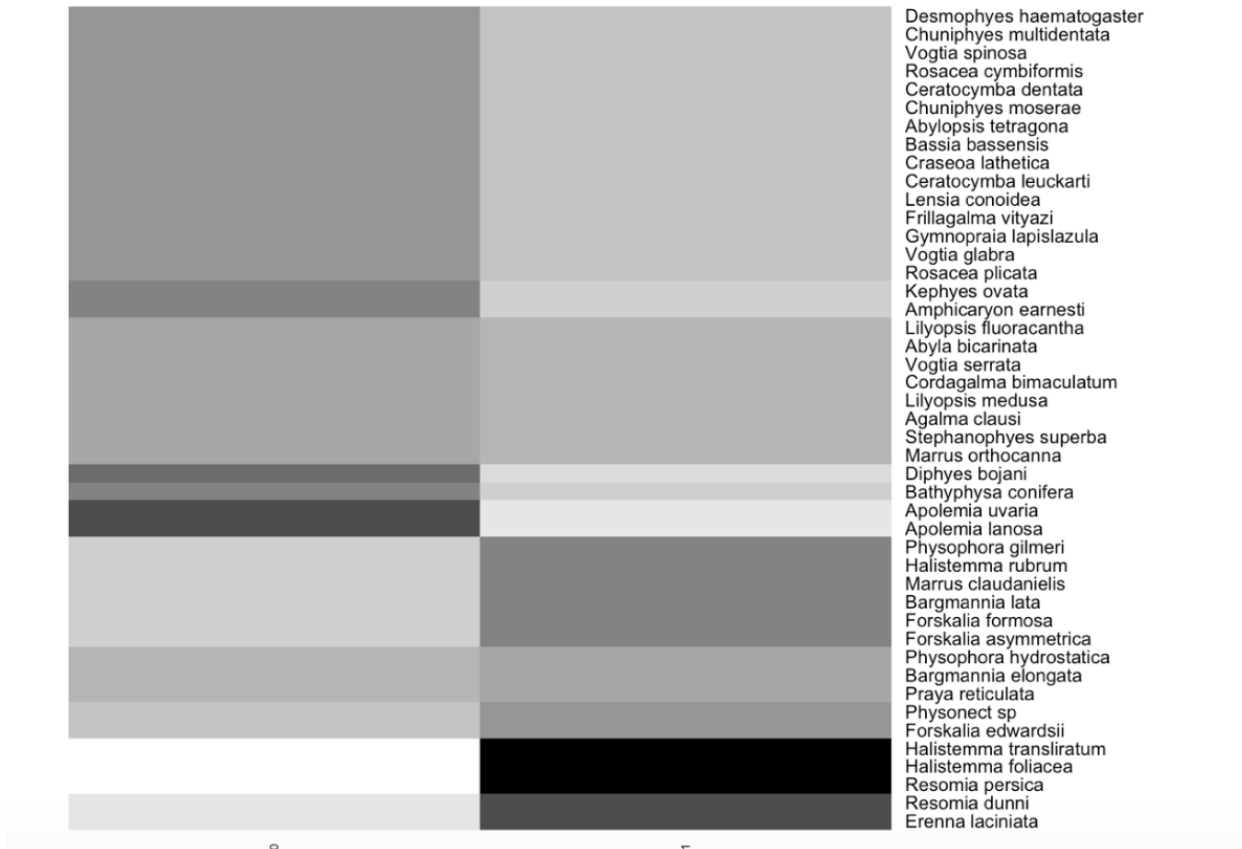
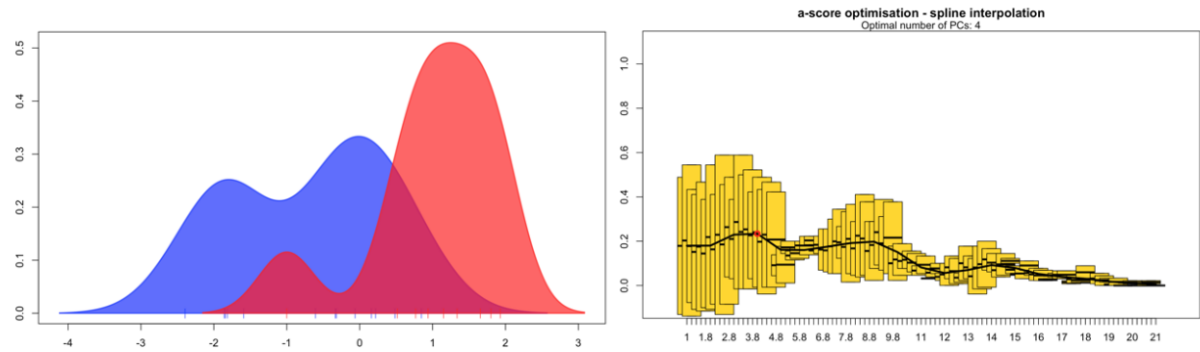


Figure 12: DAPC for fish presence in the diet. Three PCs retained after a-score optimization (100 iterations). One LDA function used. Discriminant power on training set: 68.1%. Grayscale heat map shows the posterior probability distribution of the predictions. Variable contribution (top quartile) calculated by the sum of the LDA variable loadings weighted by the eigenvalue of each LDA.



Variable contribution

	Variable contribution
Involucrum.length..um.	8.4739326
total_heteroneme_volume	2.0479062
Elastic.strand.width..um.	1.2640038
Rhopaloneme.length..um.	0.4274179
Heteroneme.volume..um3	0.4255758
haploneme_elongation	0.3530771
Desmoneme.length..um.	0.3274451
Tentacle.width..um.	0.2763979

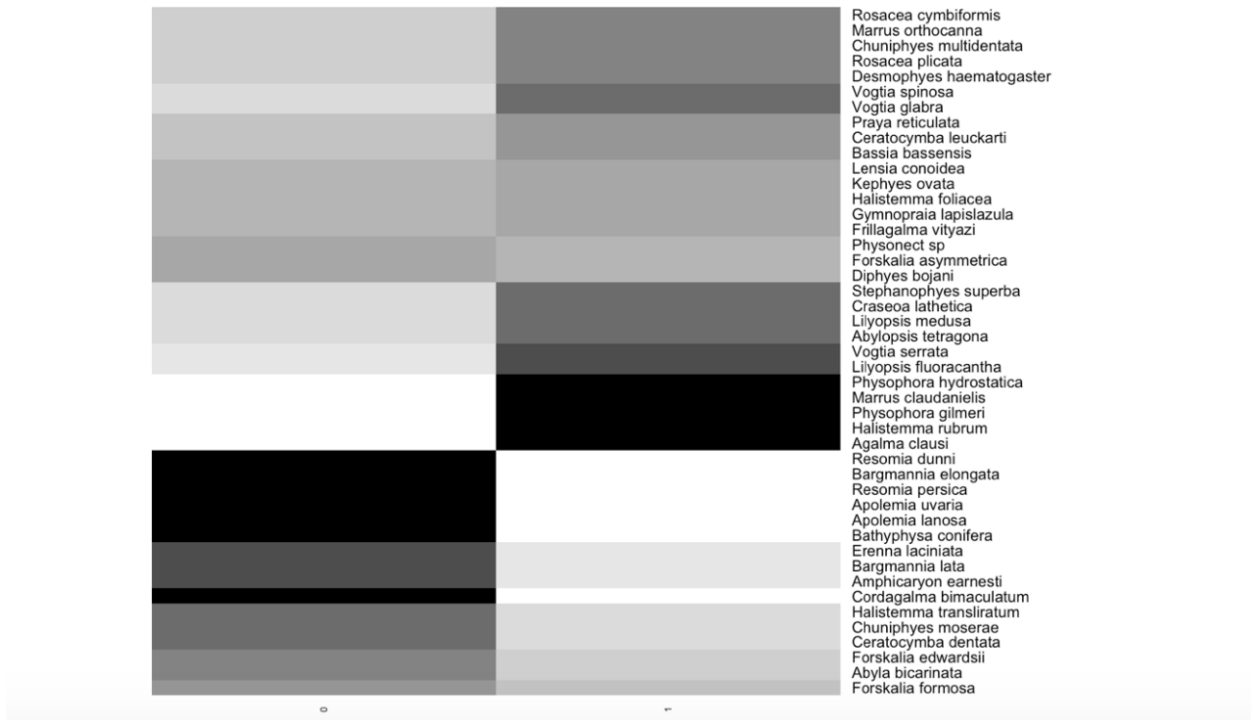


Figure 13: DAPC for large crustacean presence in the diet. Four PCs retained after a-score optimization (100 iterations). One LDA function used. Discriminant power on training set: 81.8%. Grayscale heat map shows the posterior probability distribution of the predictions. Variable contribution (top quartile) calculated by the sum of the LDA variable loadings weighted by the eigenvalue of each LDA.

Character	Prey type	Ntaxa	phyloGLM AIC	phyloGLM P	phyloglm b	GLM AIC	GLM P	GLM b
Cnidoband coiledness	Decapod diet	21	23.701	0.029	2.327	21.762	0.016	3.227
Haploneme surface area:volume	Copepod diet	21	19.143	0.017	3.246	17.355	0.017	4.631
Haploneme width μm	Copepod diet	21	18.844	0.017	-3.098	16.997	0.019	-4.417
Pedicle width μm	Copepod diet	21	22.182	0.032	-1.16	23.723	0.024	-1.437
Tentacle width μm	Copepod diet	22	22.038	0.026	-1.543	23.634	0.025	-1.505
Cnidoband length μm	Copepod diet	21	23.431	0.042	-0.864	24.178	0.025	-1.131
Cnidoband width μm	Copepod diet	21	22.887	0.035	-1.545	23.658	0.027	-1.89
Heteroneme number	Copepod diet	17	20.52	0.059	-0.718	19.615	0.03	-0.973
Total haploneme volume	Copepod diet	21	23.507	0.03	-0.581	25.232	0.031	-0.578
Total heteroneme volume	Copepod diet	17	17.156	0.032	-0.533	16.369	0.031	-0.758
Pedicle width μm	Ostracod diet	21	17.523	0.041	-1.43	15.165	0.035	-1.97
Heteroneme shaft free length μm	Copepod diet	19	23.955	0.076	-1.53	23.378	0.04	-2.16
Haploneme width μm	Fish diet	21	28.118	0.091	1.268	27.551	0.043	1.642
Tentacle width μm	Fish diet	22	28.927	0.058	0.804	28.771	0.044	0.874
Haploneme surface area:volume	Fish diet	21	28.258	0.098	-1.329	27.596	0.044	-1.768
Total haploneme volume	Ostracod diet	21	20.028	0.043	-0.619	17.733	0.046	-0.681
Heteroneme volume μm^3	Copepod diet	19	24.282	0.091	-0.521	24.297	0.046	-0.72
Pedicle width μm	Fish diet	21	28.21	0.074	0.815	27.839	0.049	0.918

Figure 14: Logistic regressions between continuous morphological characters and prey type presences. Ntaxa = number of taxa used in the analyses after removing taxa with missing diet data and inapplicable character states. phyloGLM = Phylogenetic generalized logistic regression model. GLM = Generalized logistic regression model. P = p-value. b = slope. Only cases with significant GLM fits were retained. Cells colored blue indicate phyloGLM p-value < 0.05. Cells colored green indicate GLM p-value < 0.05

76 Ordinary and phylogenetic logistic regression of morphological characters and the pres-
 77 ence/absence of prey types:

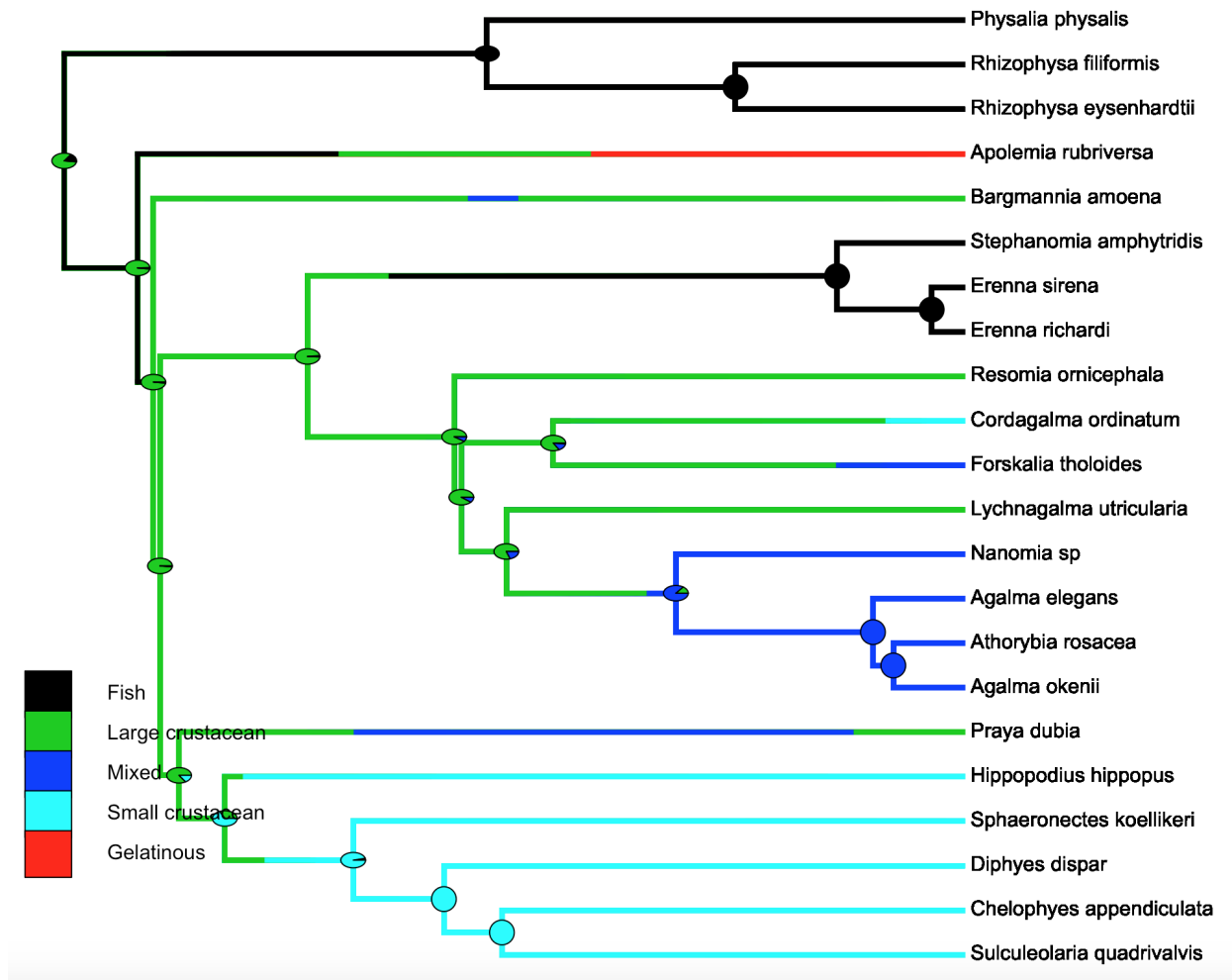


Figure 15: SIMMAP Feeding guilds.

78 Variance-Covariance Matrix analyses of phenotypic intergation and evolutionary modular-
79 ity:

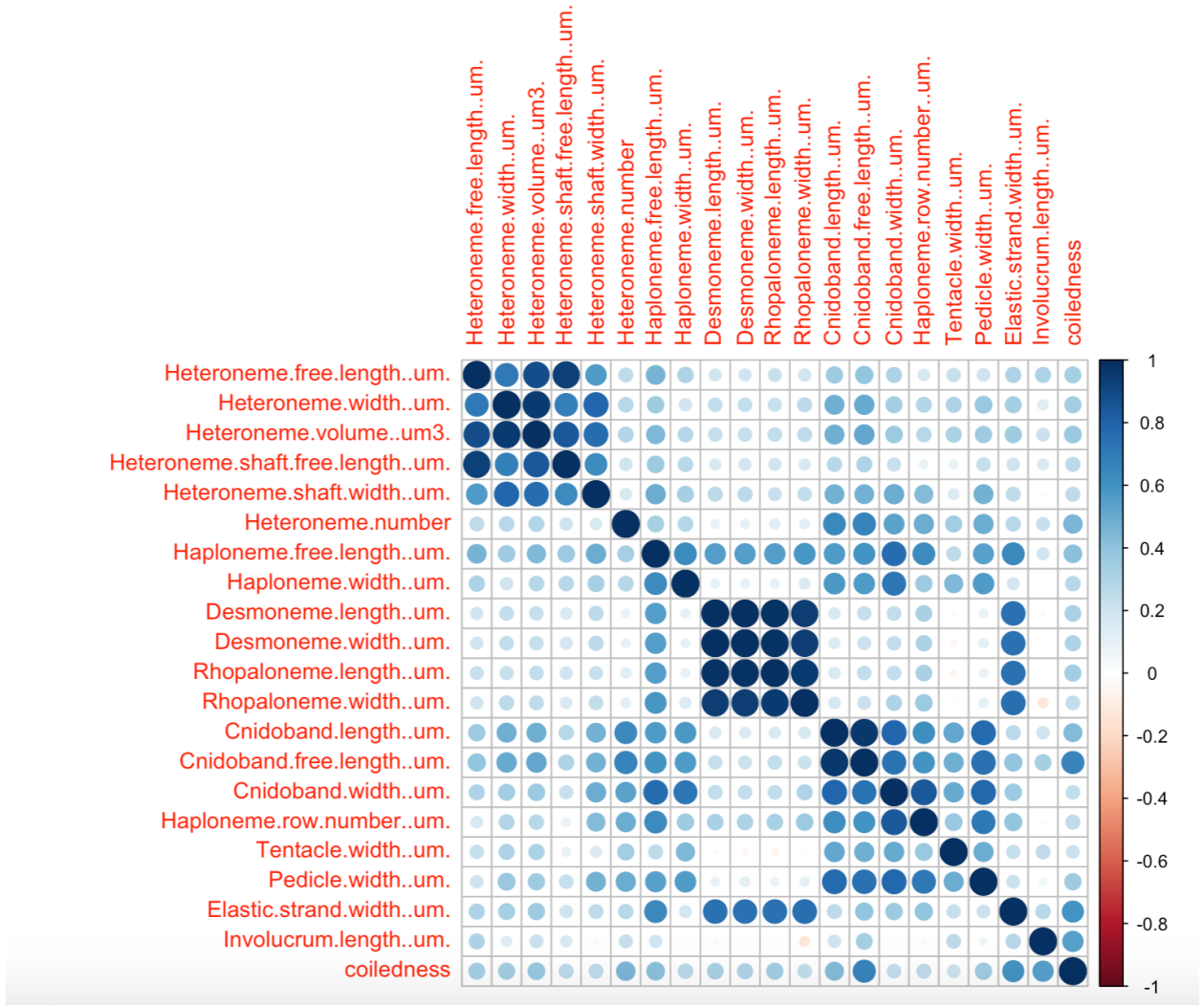


Figure 16: Rate covariance matrix for the whole tree using all taxa (45 species), transforming inapplicable states to zeroes. Covariances scaled to correlations. All characters estimated simultaneously under Brownian Motion.

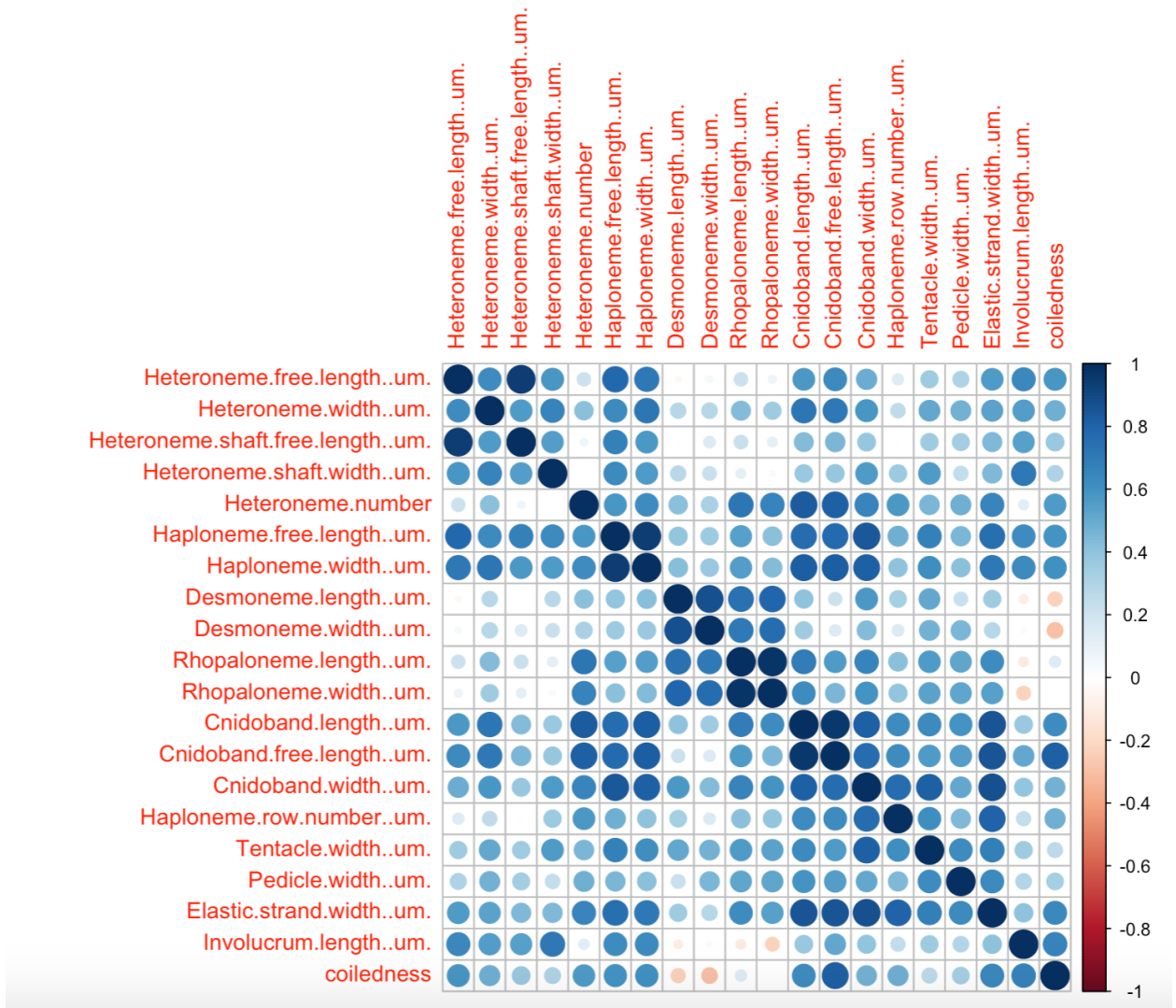


Figure 17: Rate covariance matrix for the whole tree using only taxa without inapplicable states (24 species). Covariances scaled to correlations. All characters estimated simultaneously under Brownian Motion.

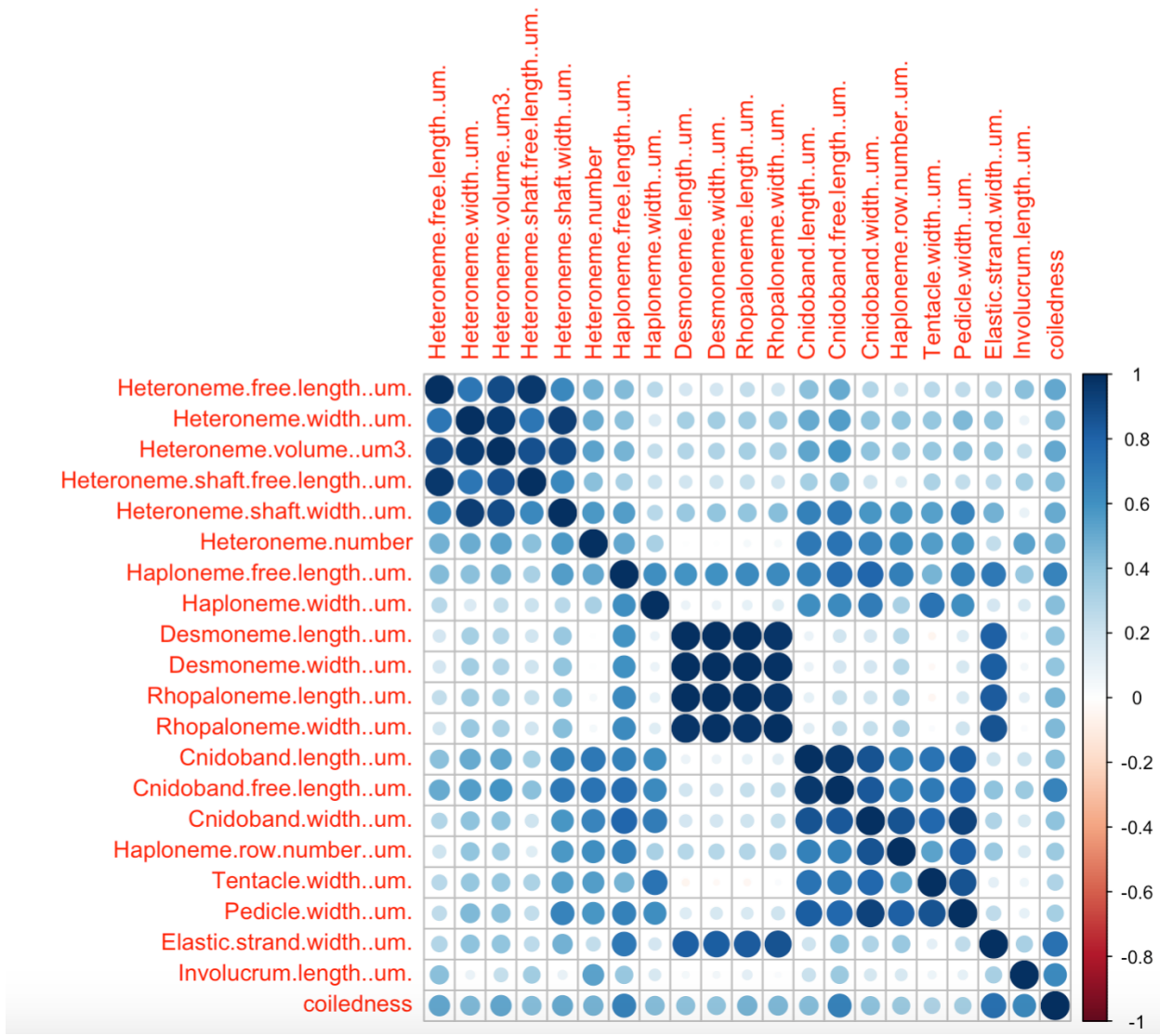


Figure 18: Rate covariance matrix for the whole tree using only taxa with diet data (22 species), transforming inapplicable states to zeroes. Covariances scaled to correlations. All characters estimated simultaneously under Brownian Motion.

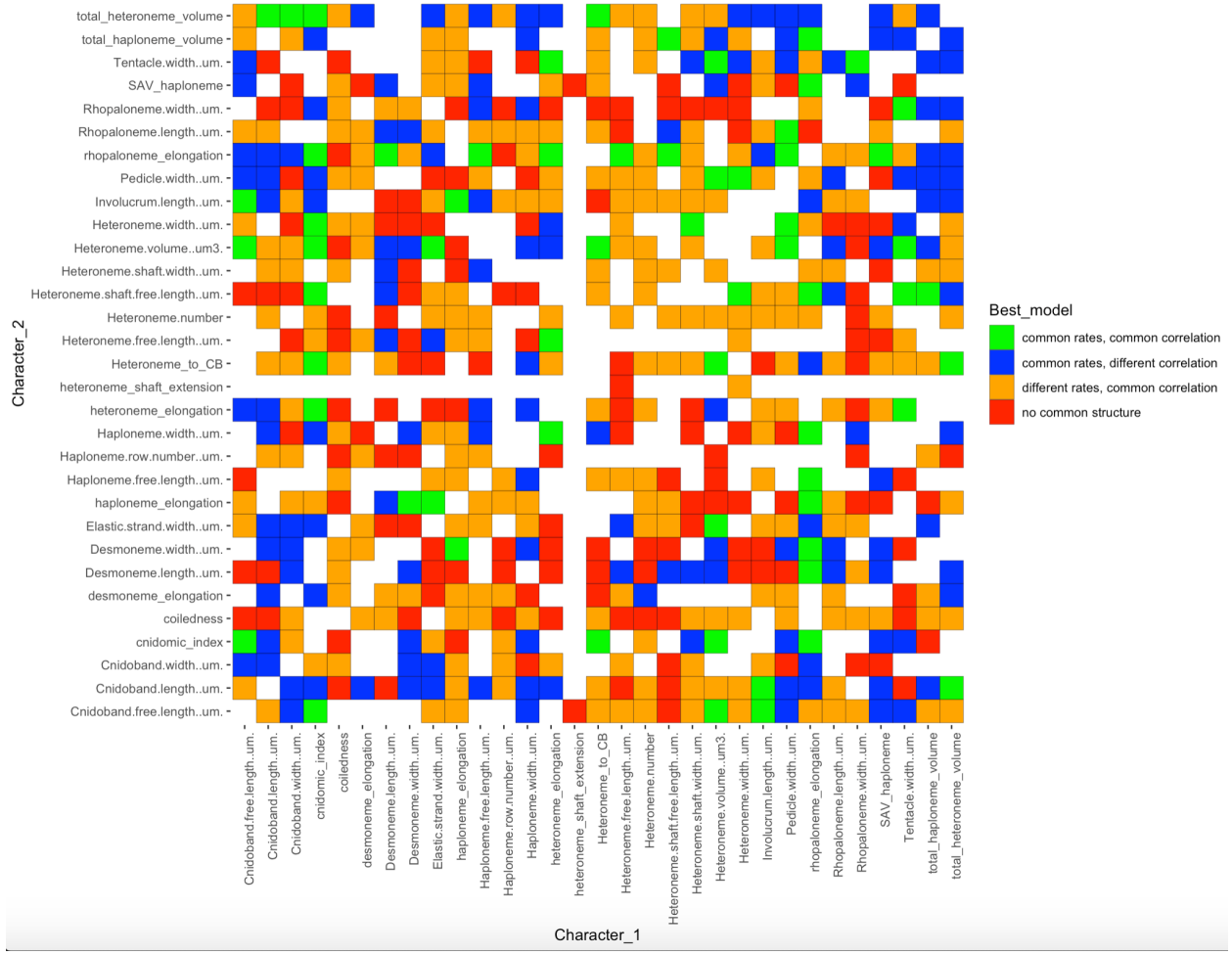


Figure 19: Best models (lowest AIC) supported in a pairwise character rate covariance analysis comparing correlated Brownian Motion models across the five selective regimes. Selective regimes were mapped onto the tree using an ancestral state reconstruction of the feeding guilds. Blank cells represent computationally singular contrasts.

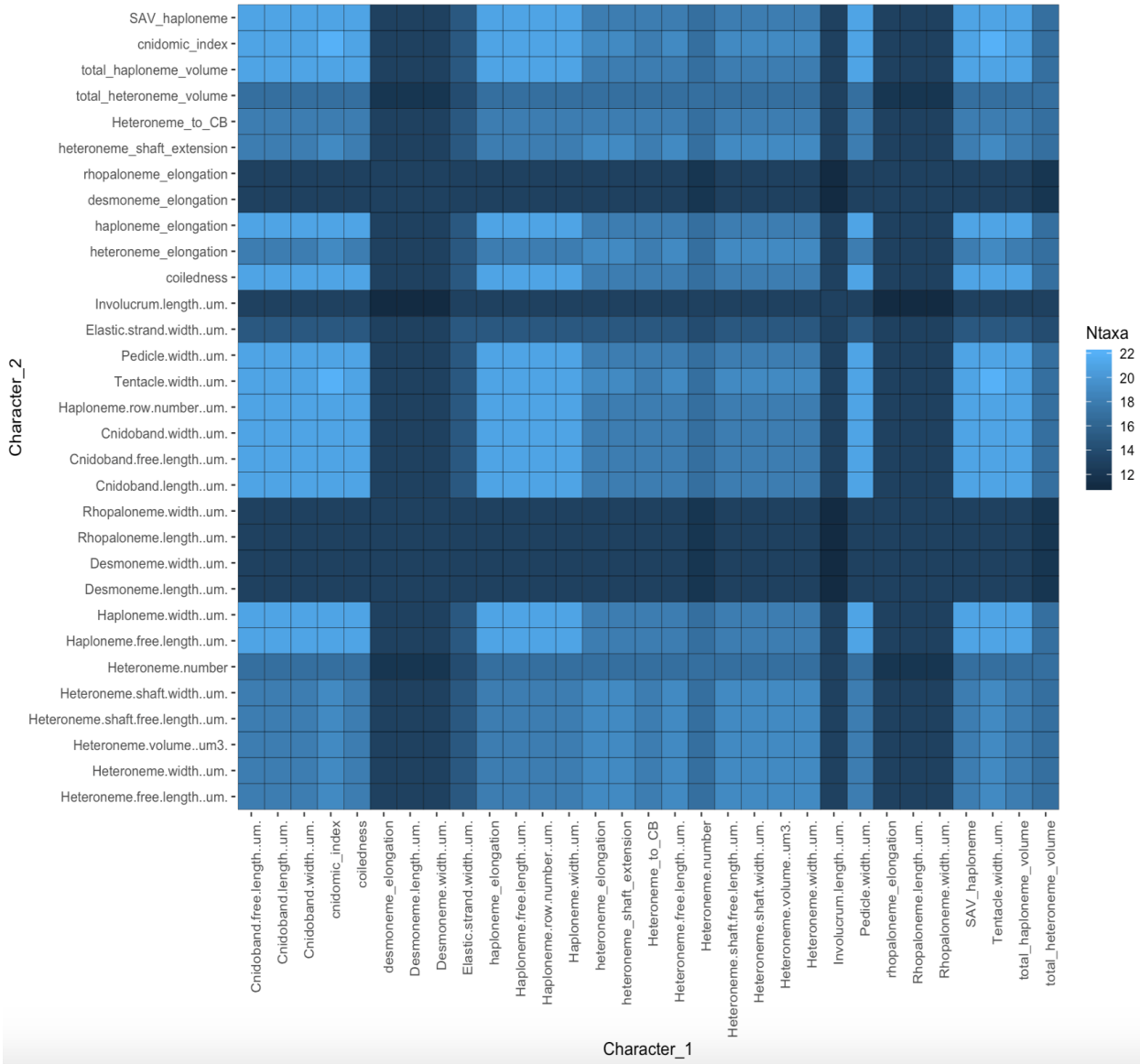


Figure 20: Number of taxa used for each pairwise contrast in the VCV analyses, given the number of taxa without inapplicable states.



Figure 21: Pairwise estimated rate covariance matrices across the five selective regimes, using only taxa with diet data. Covariances scaled to correlations. Selective regimes were mapped onto the tree (22 species with diet data) using a stochastic mapping of the feeding guilds. Tree is pruned to taxa with no inapplicable states for a given character pair. Not all regimes are represented in all contrasts. Question marks represent computationally singular contrasts.

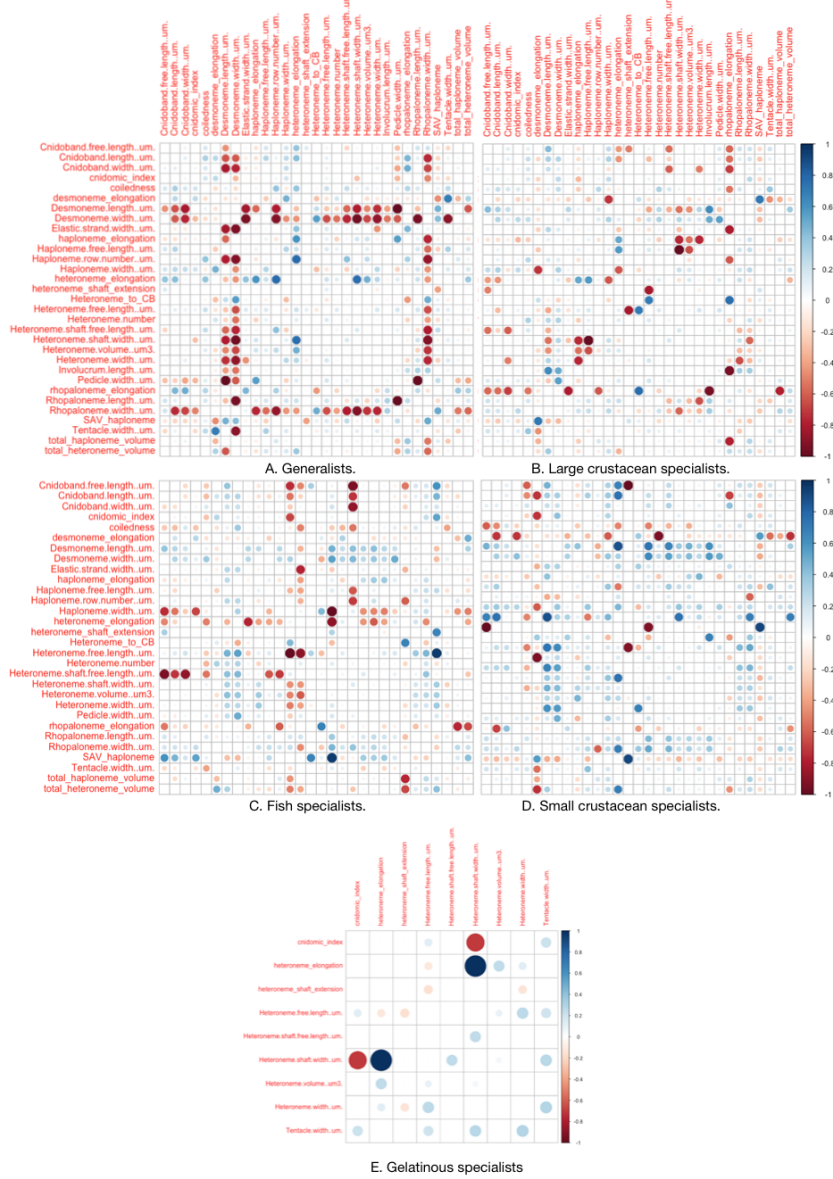


Figure 22: Scaled differences between the regime-specific covariance matrices in @ref{VCV_Regimes} and the whole tree covariance matrix.

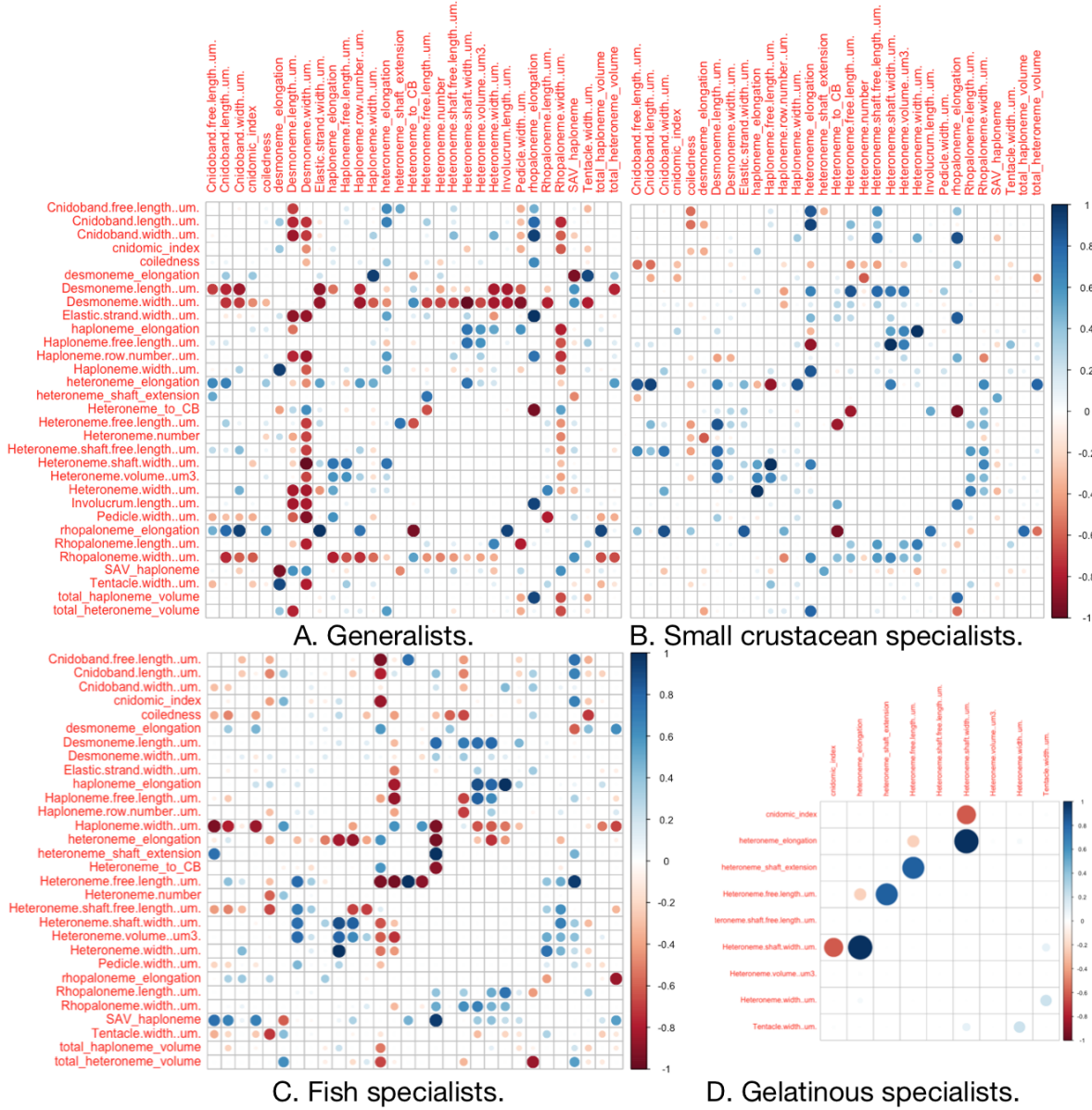


Figure 23: Scaled differences between the regime-specific covariance matrices in `@ref{VCV_Regimes}` and the covariance matrices in their preceding regime, the large-crustacean specialist regime.

80 **References**

- 81 1. Katoh K, Misawa K, Kuma K-i, Miyata T (2002) MAFFT: A novel method for rapid mul-
82 tiple sequence alignment based on fast fourier transform. *Nucleic acids research* 30(14):3059–
83 3066.
- 84 2. Nguyen L-T, Schmidt HA, Haeseler A von, Minh BQ (2014) IQ-tree: A fast and
85 effective stochastic algorithm for estimating maximum-likelihood phylogenies. *Molecular
86 biology and evolution* 32(1):268–274.
- 87 3. Kalyaanamoorthy S, Minh BQ, Wong TK, Haeseler A von, Jermiin LS (2017) Mod-
88 elFinder: Fast model selection for accurate phylogenetic estimates. *Nature methods* 14(6):587.
- 89 4. Höhna S, et al. (2016) RevBayes: Bayesian phylogenetic inference using graphical
90 models and an interactive model-specification language. *Systematic Biology* 65(4):726–736.
- 91 5. Team RC (2017) R: A language and environment for statistical computing. Vienna,
92 austria: R foundation for statistical computing; 2017.
- 93 6. Shapiro SS, Wilk MB (1965) An analysis of variance test for normality (complete
94 samples). *Biometrika* 52(3/4):591–611.
- 95 7. Pagel M (1994) Detecting correlated evolution on phylogenies: A general method for
96 the comparative analysis of discrete characters. *Proceedings of the Royal Society of London
97 Series B: Biological Sciences* 255(1342):37–45.
- 98 8. Grafen A (1989) The phylogenetic regression. *Philosophical Transactions of the Royal
99 Society of London B, Biological Sciences* 326(1233):119–157.
- 100 9. Jombart T, Devillard S, Balloux F (2010) Discriminant analysis of principal components:
101 A new method for the analysis of genetically structured populations. *BMC genetics* 11(1):94.